

OUTFLOW-DRIVEN TRANSIENTS FROM THE BIRTH OF BINARY BLACK HOLES

SHIGEO S. KIMURA^{1,2,3}, KOHTA MURASE^{1,2,3,4}, AND PETER MÉSZÁROS^{1,2,3}

¹Department of Physics, Pennsylvania State University, University Park, Pennsylvania 16802, USA

²Department of Astronomy & Astrophysics, Pennsylvania State University, University Park, Pennsylvania 16802, USA

³Center for Particle and Gravitational Astrophysics, Pennsylvania State University, University Park, Pennsylvania 16802, USA

⁴Yukawa Institute for Theoretical Physics, Kyoto, Kyoto 606-8502, Japan

ABSTRACT

We consider the electromagnetic radiation from newborn binary black holes (BBHs) formed by the evolution of isolated massive stellar binaries. Before the formation of a BBH, the binary consists of a primary black hole (BH) and a secondary Wolf-Rayet star. We investigate two types of transients from the birth of a secondary BH: one powered by the Bondi-Hoyle-Lyttleton accretion onto the primary BH, and the other induced by accretion onto the secondary BH. In the former scenario, when the secondary collapses to a BH, it may eject a fraction of its outer material, which forms a disk around the primary BH and induces an ultrafast outflow. This companion-induced outflow can lead to week-scale optical transients with a kinetic energy of $\sim 10^{47} - 3 \times 10^{48}$ erg, ejecta velocity of $10^8 - 10^9$ cm s⁻¹, and absolute magnitude ranging from about -10 to -12 . In the latter scenario, assuming that the tidal torque synchronizes the spin period of the secondary to the orbital period of the primary, the accretion of the stellar material is expected to form a disk around a newborn BH, following its core-collapse. This disk may produce an energetic outflow with a kinetic energy of $\sim 10^{52}$ erg and the outflow velocity of $\sim 10^{10}$ cm s⁻¹, resulting in an optical transient of absolute magnitude from ~ -13 to ~ -14 with a duration of a few days. While dimmer than ordinary supernovae, their light curves and late-time spectra are distinctive, and dedicated optical transient surveys could detect these two types of transients, the second type also leading to detectable radio signals.

Keywords: supernovae: general — black hole physics — binaries: close — gravitational waves — accretion, accretion disks

1. INTRODUCTION

The advanced Laser Interferometer Gravitational-wave Observatory (LIGO) revealed the existence of black holes (BH) of $\sim 30M_{\odot}$ through the detection of gravitational waves (GWs) from mergers of binary black holes (BBHs) (Abbott et al. 2016a,b,c). The formation process of BBHs is under active debate, and several models have been proposed, such as binaries of primordial black holes (e.g., Nakamura et al. 1997; Sasaki et al. 2016; Mandic et al. 2016), dynamical formation in dense stellar clusters (e.g., Sigurdsson & Hernquist 1993; Portegies Zwart & McMillan 2000; Rodriguez et al. 2016), and evolution of isolated massive stellar binaries (e.g., Tutukov & Yungelson 1993; Kinugawa et al. 2014; Belczynski et al. 2016; Marchant et al. 2016; Mandel & de Mink 2016).

Future GW observations may provide the mass, spin, and redshift distributions of merging BBHs, which are useful to probe the environments where BBHs are formed (e.g., Hotokezaka & Piran 2017, and references therein). Searching for electromagnetic (EM) coun-

terparts from merging BBHs is another way to study them. However, there is a substantial time gap, typically $\sim 0.1 - 1$ Gyr, between the stellar merger events and the formation of BBHs, which makes it difficult to probe the environments of the BBH formation. Besides, simultaneous detections of EM counterparts and GWs are not guaranteed, because possible EM signals considered so far require some specific conditions, such as the existence of a fossil disk (Perna et al. 2016; Murase et al. 2016; Kimura et al. 2017; Ioka et al. 2016), or a BBH formation in anomalously dense environments, such as the inside of very massive stars (Loeb 2016; Dai et al. 2016) or active galactic nuclei (Bartos et al. 2017; Stone et al. 2017). Instead, searching for the EM radiation from newborn BBHs would enable us more directly to probe the environment of BBH formation.

In this work, we suggest new classes of transients associated with the birth of a BBH system, which are a consequence of the evolution of the progenitor binary stellar system. The transients investigated in this work are *not coincident* with the GW emission at the BH-

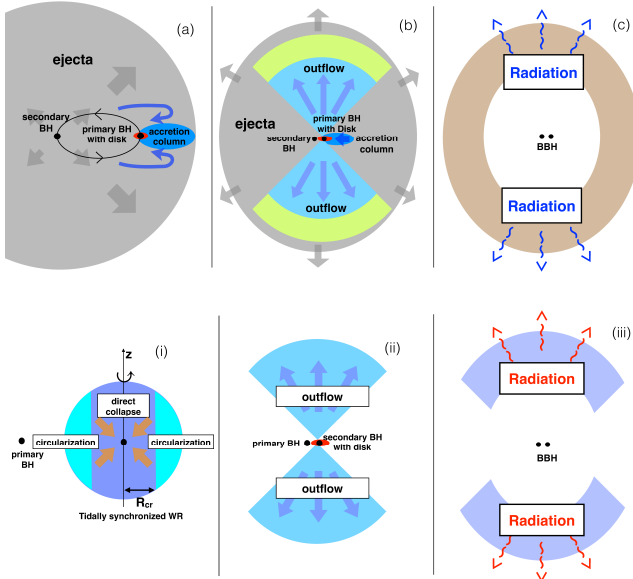


Figure 1. Schematic picture of two types of outflow-driven transients considered in this work. (Upper panel): Companion-induced accretion transients (CIATs); (a) At the birth of a BBH, a small amount of material is ejected by the secondary BH. It accretes onto the primary BH, forming a disk around the latter. (b) A disk-driven outflow is launched. (c) Thermal radiation diffusely escape from the ejecta, but a fraction of the ejecta falls back onto the primary BH. (Lower panel): Tidally-locked secondary supernovae (TLSSNe); (i) A WR is synchronized via the tidal force before its collapse. The inner part forms a secondary BH, while the outer material forms a disk around the BH. (ii) An ejecta is launched by the disk-driven outflow. (iii) Thermal photons diffuse out from the ejecta.

BH merger. Nevertheless, if they are observed, they can provide important clues about the formation scenario of BBHs. We consider two possibilities: one induced by the primary BHs, and the other powered by the secondary BHs. We describe the basic binary evolution process and the two possible outcomes in Section 2. We discuss the time evolution and observational features of the companion-induced transient in Section 3, and the corresponding discussion of the transient resulting from a tidally-locked secondary is given in Section 4. In Section 5 we summarize our results and the conclusions concerning observational prospects. Throughout this work, we use the notation of $A = A_x 10^x$.

2. CONSEQUENCES OF THE EVOLUTIONARY SCENARIO

According to the isolated binary evolution models (e.g. [Belczynski et al. 2016](#)), the heavier primary collapses to a BH earlier than the secondary, which forms a BH and main-sequence star binary. When the secondary evolves to a giant star, the binary separation decreases considerably during a common envelope evolution ([Paczynski](#)

[1976; Webbink 1984](#)). After that, the secondary is expected to be a Wolf-Rayet star (WR) following the envelope ejection, and the BH-WR binary becomes a BBH after the gravitational collapse of the WR (e.g. [Dominik et al. 2012](#)).

At the end of the binary evolution, after the massive secondary star has collapsed and the BBH has formed, its subsequent fate depends on the angular momentum of the secondary star. Although the angular momentum distribution of the secondary is highly uncertain, the spin of the secondary star may be tidally locked in a close binary system ([Zahn 1977; Tassoul 1987](#)). [Kushnir et al. \(2016\)](#) give the synchronization time as,

$$t_{\text{TL}} \sim 10^7 \left(\frac{t_{\text{mer}}}{1 \text{ Gyr}} \right)^{17/8} \text{ yr}, \quad (1)$$

where $t_{\text{mer}} = 5c^5 a^4 / (512G^3 M_*^3) \sim 3.2 \times 10^9 a_{12}^4 M_{*,1}^{-3}$ yr is the GW inspiral time, M_* is the primary mass, and a is the binary separation. We assume the mass ratio $q = 1$ for simplicity and use $M_* \sim 10M_\odot$ and $a \sim 10^{12}$ cm for the purposes of an estimate, which indicates that t_{TL} is longer than the typical lifetime of massive stars, $t_{\text{life}} \sim 10^6$ yr. However, for a high mass $M_* \sim 30 M_\odot$ or small separation $a \sim 5 \times 10^{11}$ cm, $t_{\text{TL}} < t_{\text{life}}$ is possible. We caution that this timescale has significant uncertainties caused by the strong dependence on the detailed stellar structure, especially the size of the convective region ([Kushnir et al. 2016](#)). The size of the star also affects this timescale.

When $t_{\text{TL}} > t_{\text{life}}$, the secondary spin is expected to be slow enough for the secondary star to collapse directly into a BH. However, even in such cases, the sudden gravitational potential change may lead to a weak explosion ([Nadezhin 1980](#)). Although the explosion itself is very dim, brighter transients may be caused by the primary BH if the binary separation is sufficiently small. A fraction of the ejecta of the weak explosion should be gravitationally captured by the primary BH via Bondi-Hoyle-Littleton accretion ([Hoyle & Lyttleton 1939; Bondi 1952](#)). This accreting material forms a disk around the primary, which results in a powerful outflow ([Ohsuga et al. 2005](#)). This outflow injects a considerable amount of energy into the rest of the ejecta, leading to a Companion-Induced Accretion Transient (CIAT).

In the opposite case when $t_{\text{TL}} < t_{\text{life}}$, the spin of the secondary can be tidally synchronized (cf. [Detmers et al. 2008; Yoon et al. 2010](#)). In this case, the outer material of the secondary star has sufficient angular momentum to form a disk as it gravitationally collapses. The disk is massive enough to produce a powerful outflow, which results in a Tidally-Locked Secondary Supernova (TLSSN). The kinetic energy of this outflow is so high as to result in a bright radio afterglow.

Schematic outlines of CIATs and TLSSNe are shown in Figure 1. Optical transients caused by the disk-driven outflow have been considered in the context of single BH formation (Kashiyama & Quataert 2015) and BH mergers (Murase et al. 2016). CIATs and TLSSNe provide different examples associated with a newborn BBH.

3. COMPANION-INDUCED-ACCRETION TRANSIENTS FROM BBH FORMATION (BBH-CIATs)

3.1. CIATs

We consider a massive binary system consisting of a primary BH and a secondary WR. The binary parameters are: the secondary mass WR $M_* = 10 M_\odot$, the WR radius $R_* = 10^{11.5}$ cm¹, separation $a = 10^{12}$ cm, and the primary mass M_{BH} . Hereafter, we fix $M_{\text{BH}} = M_*$ for simplicity. The orbital velocity of the BH is $v_{\text{orb}} = \sqrt{GM_*/(2a)} \simeq 4.6 \times 10^7 M_{*,1}^{1/2} a_{12}^{-1/2}$ cm s⁻¹. When the WR collapses to a BH, its outer material of mass $M_{\text{ej}} \sim 10^{-2} M_\odot$ may be ejected (Kashiyama, private communication). The ejecta velocity is comparable to the escape velocity,

$$V_{\text{ej},i} \approx \xi V_{\text{esc}} = \xi \sqrt{\frac{2GM_*}{R_*}} \quad (2)$$

$$\simeq 1.8 \times 10^8 M_{*,1}^{1/2} R_{*,11.5}^{-1/2} \xi_{0.3} \text{ cm s}^{-1},$$

where $\xi \sim 2$ is a correction factor relative to the escape velocity. This ejecta velocity is always higher than the orbital velocity. The kinetic energy of the ejecta is estimated to be

$$\mathcal{E}_{\text{ej},i} = \frac{1}{2} M_{\text{ej}} V_{\text{ej},i}^2 \simeq 3.3 \times 10^{47} M_{*,1} R_{*,11.5}^{-1} M_{\text{ej},-2} \xi_{0.3}^2 \text{ erg}, \quad (3)$$

This expelled ejecta amounts to an explosion energy comparable to the gravitational energy loss due to the neutrino radiation (Nadezhin 1980; Lovegrove & Woosley 2013).

We assume that the ejecta is in homologous expansion. The density profile inside the ejecta is often parameterized through a power-law form with index 0–1 (e.g. Li & Paczyński 1998; Kasen & Bildsten 2010). We assume a uniform density (index = 0) for simplicity. The velocity profile inside the homologously expanding ejecta is written as $V(R) = R/t'$ ($t' = 0$ is the time when the secondary collapses). During the expansion, as the velocity at fixed radius decreases with time,

¹ The radii of WR stars are somewhat uncertain. An atmospheric model suggests $R_* \sim 2 \times 10^{11}$ cm (Crowther 2007). Stellar evolution models predict a relation $R_* \sim 7 \times 10^{10} (M_*/10 M_\odot)^{0.7}$ cm (Schaerer & Maeder 1992; Kushnir et al. 2016), while a binary evolution model shows that the radius is larger for lighter secondaries, $R_* \sim 10^{12}$ cm for $M_* \sim 5 M_\odot$ (Yoon et al. 2010).

the gas that has a velocity lower than V_{esc} cannot escape to infinity. We can introduce a threshold velocity, $V_{\text{thr}} = V_{\text{esc}} \chi' = V_{\text{esc}} \sqrt{1 - R_*/a}$, such that the material with $V(R_*) < V_{\text{thr}}$ is not ejected and falls back into the secondary. Note that for this threshold velocity, all the material that can reach the position of the primary is ejected. Then, the density of the ejecta at $R = a$ can be expressed as

$$\rho_{\text{ej},m} \approx \frac{3M_{\text{ej}}}{4\pi a^3} \left(\frac{t'}{t_{\text{arr}}} \right)^{-3} (\Theta(V_{\text{ej},i} t' - a) - \Theta(V_{\text{thr}} t' - a)), \quad (4)$$

where $\Theta(x)$ is the Heaviside step function and $t_{\text{arr}} = a/V_{\text{ej},i}$ is the arrival time of the ejecta at the primary position. The fraction of the fallback matter is small, $M_{\text{fb}}/M_{\text{ej}} \approx (V_{\text{thr}}/V_{\text{ej},i})^3 \simeq 7.1 \times 10^{-2}$.

After $t' > t_{\text{arr}}$, the ejecta accretes onto the primary BH. Assuming that the sound speed in the ejecta is small due to adiabatic expansion, the accretion radius is $R_{\text{acc}} = GM_{\text{BH}}/(V_a^2 + v_{\text{orb}}^2) \approx GM_{\text{BH}}/V_a^2$, where $V_a = a/t$ is the ejecta velocity at $R = a$ (Edgar 2004). Since $R_{\text{acc}} < a$ is satisfied, we can estimate the accretion rate to be given by the Bondi-Hoyle-Lyttleton rate (Shima et al. 1985; Edgar 2004)

$$\dot{M}_{\text{B-H}} \approx 4\pi R_{\text{acc}}^2 \rho_{\text{ej},m} \sqrt{V_a^2 + v_{\text{orb}}^2} \quad (5)$$

$$\simeq 8.7 \times 10^{-9} M_{*,1}^{1/2} R_{*,11.5}^{3/2} M_{\text{ej},-2} a_{12}^{-3} \xi_{0.3}^3 M_\odot \text{ s}^{-1}.$$

This accretion rate is constant in time, and much higher than the Eddington accretion rate. The duration of this high accretion rate is

$$t_{\text{dur}} = t'_{\text{stop}} - t'_{\text{arr}} \simeq 7.7 \times 10^3 M_{*,1}^{-1/2} R_{*,11.5}^{1/2} a_{12} \chi_{-0.16} \text{ s}, \quad (6)$$

where $t'_{\text{stop}} = a/V_{\text{thr}}$ and $\chi = (\xi - \chi')/(\xi \chi') \simeq 0.7$ for the reference parameters. After this time, the accretion stops because there is no gas around the primary due to the fallback. The total accreted mass, $M_{\text{acc}} \approx \dot{M}_{\text{B-H}} t_{\text{dur}} \simeq 6.7 \times 10^{-5} R_{*,11.5}^{3/2} M_{\text{ej},-2} a_{12}^{-3/2} \xi_{0.3}^{-3} \chi_{-0.16} M_\odot$, is much smaller than M_{ej} .

The accreted gas, due to its orbital angular momentum, forms a disk surrounding the primary BH (de Val-Borro et al. 2009; Huarte-Espinosa et al. 2013), and this accretion disk leads to a powerful outflow owing to its high accretion rate (Ohsuga et al. 2005; Jiang et al. 2014). We assume that the outflow is almost isotropic, a fraction $\eta_w \sim 1/3$ of the accreted material going into the outflow, whose velocity is approximately constant, $V_w \sim 10^{10}$ cm s⁻¹. These values of η_w and V_w are consistent with recent radiation magnetohydrodynamic calculations (Takahashi & Ohsuga 2015; Narayan et al. 2017). The luminosity and total energy

of the outflow are

$$L_w \approx \frac{1}{2} \eta_w \dot{M}_{\text{B-H}} V_w^2 \simeq 2.7 \times 10^{44} M_{*,1}^{1/2} R_{*,11.5}^{3/2} \times M_{\text{ej},-2} a_{12}^{-3} \xi_{0.3}^{-3} \eta_{-0.5} V_{10}^2 \text{ erg s}^{-1}, \quad (7)$$

$$\mathcal{E}_w \approx L_w t_{\text{dur}} \simeq 2.1 \times 10^{48} R_{*,11.5}^2 M_{\text{ej},-2} \times a_{12}^{-2} \xi_{0.3}^{-3} \chi_{-0.16} \eta_{-0.5} V_{10}^2 \text{ erg.} \quad (8)$$

Note that although the opening angle of the outflow is large, it is not isotropic and probably does not cover the entire solid angle (see panel (b) of Figure 1). We assume that the mass accretion onto the BH is not quenched by the outflow.

As the material accretes onto the BH through an accretion column behind the BH, the accretion disk is covered by the ejecta before producing the outflow (see the panel (a) of Figure 1). Thus, the outflow is, at least initially, confined within the ejecta. The outflow injects a considerable amount of kinetic energy into the ejecta, and accelerates it. For $t < t_{\text{dur}}$ ($t = t' - t'_{\text{arr}}$), during which the outflow is produced, the ejecta velocity is estimated to be $V_{\text{ej}} \approx \sqrt{L_w t / M_{\text{ej}}} \propto t^{1/2}$, and the ejecta radius is $R_{\text{ej}} = \int V_{\text{ej}} dt \approx 2V_{\text{ej}} t / 3$. The balance between adiabatic loss and energy injection determines the total internal energy of the ejecta. Assuming all the kinetic energy of the outflow is converted into radiation energy in the ejecta (see the next subsection), we obtain $\mathcal{E}_{\text{int}} / t_{\text{dyn}} \sim L_w$, where $t_{\text{dyn}} = R_{\text{ej}} / V_{\text{ej}}$. This leads to $\mathcal{E}_{\text{int}} \approx 2L_w t / 3$. Then, the temperature evolves as $T_{\text{ej}} \sim (\mathcal{E}_{\text{int}} / (a_r R_{\text{ej}}^3))^{1/4} \propto t^{-7/8}$, where a_r is the radiation constant. Although the bulk of photons are trapped inside the ejecta, a small fraction of photons can diffuse out from the surface of the ejecta. This photon diffusion luminosity evolves as $L_{\text{ph}} \sim \mathcal{E}_{\text{int}} / t_{\text{ph}} \propto t^{5/2}$, where $t_{\text{ph}} \approx R_{\text{ej}} \tau / c \sim M_{\text{ej}} \kappa / (c R_{\text{ej}})$, where $\tau \approx \rho \kappa R_{\text{ej}}$ and κ is the opacity.

When the outflow stops at $t = t_{\text{dur}}$, the temperature is estimated to be

$$T_{\text{ws,c}} \approx \left(\frac{27 \mathcal{E}_w}{16 \pi a_r V_{\text{ej},c}^3 t_{\text{dur}}^3} \right)^{0.25} \simeq 1.4 \times 10^6 M_1^{3/8} R_{*,11.5}^{-5/8} \times a_{12}^{-1/2} M_{\text{ej},-2}^{1/4} \xi_{0.3}^{3/8} \chi_{-0.16}^{-7/8} \eta_{-0.5} V_{10}^{-1/4} \text{ K.} \quad (9)$$

Since the total outflow energy is higher than the initial ejecta energy, a shock breakout is expected at $t \lesssim t_{\text{dur}}$ (Matzner & McKee 1999). For $t > t_{\text{dur}}$, the ejecta velocity is constant, $V_{\text{ej},c} \approx \sqrt{2\mathcal{E}_w / M_{\text{ej}}}$, and the radius is $R_{\text{ej}} \approx V_{\text{ej},c} t$. In this phase, there is a cavity inside ejecta, so the density is written as $\rho_{\text{ej}} \approx M_{\text{ej}} / (4\pi R^2 H) \propto t^{-3}$, where $H \propto R_{\text{ej}}$ is the thickness of the ejecta². The

ejecta is adiabatically expanding, which makes $T_{\text{ej}} \propto \rho_{\text{ej}}^{1/3} \propto t^{-1}$. The luminosity of diffusing photons is then constant for time, $L_{\text{ph}} \sim R_{\text{ej}}^3 a_r T_{\text{ej}}^4 / t_{\text{ph}} \propto t^0$. This phase continues until the radiation breakout time by which the bulk of photons escape from the ejecta,

$$t_{\text{bo,c}} \approx \sqrt{\frac{\kappa M_{\text{ej}}}{4\pi c V_{\text{ej},c}}} \simeq 1.5 \times 10^5 R_{*,11.5}^{-1/2} \times a_{12}^{1/2} M_{\text{ej},-2}^{1/2} \xi_{0.3}^{3/4} \chi_{-0.16}^{-1/4} \eta_{-0.5}^{1/2} V_{10}^{1/2} \text{ s,} \quad (10)$$

where we use $\kappa \simeq 0.2 \text{ cm}^2 \text{ g}^{-1}$ that corresponds to fully ionized helium. The temperature and luminosity at the radiation breakout time is computed as

$$T_{\text{bo,c}} \approx \left(\frac{V_{\text{ej,c}} t_{\text{dur}}}{R_{\text{bo,c}}} \right) T_{\text{ws,c}} \simeq 4.6 \times 10^4 M_{*,1}^{-1/8} R_{*,11.5}^{3/8} \times M_{\text{ej},-2}^{-1/4} \xi_{0.3}^{-3/8} \chi_{-0.16}^{3/8} \eta_{-0.5}^{5/8} V_{10}^{5/4} \text{ K,} \quad (11)$$

$$L_{\text{ph,c}} \approx \frac{4\pi R_{\text{bo,c}}^3 a_r T_{\text{bo,c}}^4}{3\kappa t_{\text{bo,c}}} \simeq 3.1 \times 10^{41} M_{*,1}^{-1/2} R_{*,11.5}^{7/2} \times a_{12}^{-2} \xi_{0.3}^{-9/2} \chi_{-0.16}^{5/2} \eta_{-0.5}^{3/2} V_{10}^3 \text{ erg s}^{-1}, \quad (12)$$

where $R_{\text{bo,c}} = V_{\text{ej,c}} t_{\text{bo,c}}$. For $t > t_{\text{bo,c}}$, the photon diffusion determines the internal energy, $d\mathcal{E}_{\text{int}} / dt \sim \mathcal{E}_{\text{int}} / t_{\text{ph}}$. Then, the internal energy decays as $\exp(-t^2 / (2t_{\text{bo,c}}^2))$, so both T_w and L_{ph} decreases rapidly. We show the evolution of L_{ph} and T_{ej} in the upper panel of Figure 2.

We plot the UV (150 nm), U band (365 nm), and R band (658 nm) absolute AB magnitudes in the lower panel. Since the optical depth $\tau_{\text{ej}} > 1$ is satisfied for the times of interest, we use the Planck spectra corresponding to T_{ej} . The peak magnitude and duration are around -11 and 3 days for U band, respectively, with weaker flux and longer durations for the longer wavelength. These light curves indicate that we could distinguish these transients from usual SNe by means of their bluer color and shorter duration. Spectroscopic observations can also discriminate them from macronovae/kilonovae, since CIATs will show strong helium lines while macronovae/kilonovae will not show them.

The existence of this type of transient requires some tuning. For CIATs to occur, $\mathcal{E}_w > \mathcal{E}_{\text{ej,i}}$ should be satisfied, a condition which breaks down for models with R_* a few times smaller, larger a , higher ξ , or lower V_w than the reference model. In these cases, we expect instead the result to be failed SNe, which are much dimmer than CIATs (see the next subsection). Considering models with higher \mathcal{E}_w would be a bit extreme, since the reference model is fairly optimistic. Besides, M_* should be around $10 M_\odot$ because tidal synchronization might

² Note that ρ_{ej} is different from $\rho_{\text{ej,m}}$ that represents the ejecta

density that is not accelerated by the outflow.

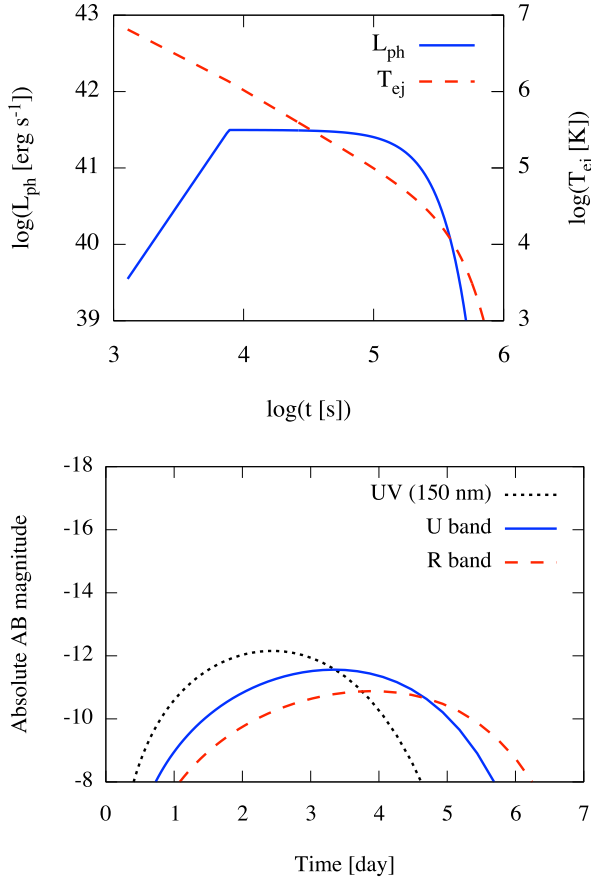


Figure 2. Time evolution of physical quantities for the CIAT model. The upper panel shows the bolometric luminosity L_{ph} (blue-solid) and the ejecta temperature T_{ej} (red-dashed). The lower panel shows absolute AB magnitudes for the UV range (150 nm, black-dotted), U band (blue-solid), and R band (red-solid).

take place for higher M_* , and a BH is not formed for lower M_* . Models with lower η_w and higher or lower M_{ej} are also possible. For these models, $t_{\text{bo},c}$ could be longer or shorter depending on the value of M_{ej} , $T_{\text{bo},c}$ does not change much owing to the weak dependence on these parameters, and L_w could be lower proportional to $\eta_w^{3/2}$.

For the nominal parameters adopted, one may expect an event rate for these peculiar SNe-like transients similar to the LIGO event rate, $9 - 240 \text{ Gpc}^{-3} \text{ yr}^{-1}$ (Abbott et al. 2016a). We expect $\sim 0.1 - 2$ events within 200 Mpc in a year, which leads to peak apparent magnitudes of these objects of $\sim 24 - 25$. Thus, they may not be seen by current optical transient surveys with detection limits of ~ 21 mag, such as the Panoramic Survey Telescope & Rapid Response System (Pan-STARRS; Hodapp et al. 2004), the Palomar Transient Factory (PTF; Law et al. 2009), and the Kiso Supernova Survey (KISS; Morokuma et al. 2014). On the

other hand, future projects with detection limits ~ 25 , such as the Large Synoptic Survey Telescope (LSST, LSST Science Collaboration et al. 2009), would be able to detect CIATs.

3.2. Failed SNe

In the cases where $\mathcal{E}_w < \mathcal{E}_{\text{ej},i}$, taking for example a separation $a \simeq 3 \times 10^{12} \text{ cm}$ and the other parameters the same as the reference values, CIATs are less important although the energy injection still helps a transient brighter; instead a weak explosion with the initial ejecta energy of Equation (3) may occur. We assume the initial internal energy of the ejecta is similar to $\mathcal{E}_{\text{ej},i}$. The radiation breakout time is

$$t_{\text{bo}} \approx \sqrt{\frac{3\kappa M_{\text{ej}}}{4\pi c V_{\text{ej},i}}} \simeq 4.2 \times 10^5 M_{*,1}^{-1/4} R_{*,11.5}^{1/4} M_{\text{ej},-2}^{1/2} \xi_{0.3}^{-1/2} \text{ s.} \quad (13)$$

Considering an adiabatic evolution, the temperature at the radiation breakout time is

$$T_{\text{bo},f} = T_{\text{ini}} \frac{R_{\text{bo},f}}{R_*} \simeq 1.8 \times 10^4 R_{*,11.5}^{1/4} M_{\text{ej},-2}^{-1/4} \text{ K,} \quad (14)$$

where $R_{\text{bo},f} \approx t_{\text{bo},f} V_{\text{ej},i}$ is the breakout radius and $T_{\text{ini}} \sim (3\mathcal{E}_{\text{ej},i}/(4\pi a_r R_*))^{1/4}$ is the initial ejecta temperature. The luminosity is then

$$L_{\text{bo},f} \approx \frac{4\pi R_{\text{bo},f}^3 a_r T_{\text{bo},f}^4}{3t_{\text{bo},f}} \simeq 3.3 \times 10^{39} M_{*,1} \xi_{0.3}^2 \text{ erg s}^{-1}. \quad (15)$$

This is dimmer than CIATs by more than an order of magnitude. Such failed SNe could however be more luminous (Moriya et al. 2010) if some amount of radioactive nuclei are produced or are included inside the ejecta.

3.3. CIAT Parameter Dependence

Although for simplicity we have used a spherically symmetric formulation, there are substantial non-spherical effects possible in this system. One is the effect of the finite binary separation, which means that the position of the outflow source is not located at the center of the ejecta. This might affect the initial evolution of the ejecta, whose quantitative discussion would probably be subject to change. Another is the effect of the outflow. We assumed some tuning so that the opening angle is wide enough that we can approximate it as spherically symmetric, while the outflow is not completely isotropic so that the ejecta density profile at the midplane does not change much. In reality, the outflow from an accretion flow might be more bipolar-like (Sadowski et al. 2014; Takahashi et al. 2016). The ejecta density profile is also probably affected by the outflow, so that the accretion rate might be modified. It is beyond the scope of this paper to investigate these effects, which would require 3-dimensional radiation hydrodynamic (3d-RHD) calculations.

We assumed for simplicity that all the kinetic energy of the outflow is converted into the radiation energy of the ejecta. We discuss the validity of this assumption. The outflow kinetic energy is first converted to the thermal energy of protons at the reverse shock. The electrons inside the shocked region are heated up by Coulomb collisions and other plasma processes. When the electrons become energetic enough, the bremsstrahlung cooling time becomes shorter than the Coulomb loss timescale (Takahara & Kusunose 1985). In addition, the Compton cooling is also efficient for the relativistic electrons. If we consider only the Coulomb heating in the far downstream, the electron temperature may be around $k_B T_e \sim m_e c^2$. Then, the energy loss time of the protons due to Coulomb losses can be estimated to be (Takahara & Kusunose 1985; Kimura et al. 2014) $t_{\text{cool}} \approx \frac{m_p}{m_e} \frac{1}{\rho_{\text{ps}} \kappa c \ln \Lambda} \simeq 1.3 \times 10^3 M_{*,1}^{-3/2} R_{*,11.5}^{3/2} a_{12}^3 M_{\text{ej},-2} \chi_{-0.16}^3 V_{10}^3$ s, where ρ_{ps} is the density in the post shock region and $\ln \Lambda \sim 30$ is the Coulomb logarithm. Here, setting $t = t_{\text{dur}}$, we have used $\rho_{\text{ps}} \sim L_w / (2\pi R_{\text{ws}}^2 V_w^3)$. Because $t_{\text{cool}} < t_{\text{dyn}} = 2t_{\text{dur}}/3$ is satisfied at $t = t_{\text{dur}}$, the outflow kinetic energy can be converted into radiation energy. In reality, the Compton cooling can also be relevant, so that the cooling of electrons may be stronger than the above estimate.

We also assume that the circularization radius of the accreted material is not large. Otherwise, if the circularization radius is too large, a considerable amount of gas could escape from the accretion disk as an outflow before arriving near the primary BH (Hashizume et al. 2015). This may reduce the net accretion rate, causing the CIATs to be fainter.

There could be other CIATs throughout the life of a BH-massive star binary. One possibility arises during the common envelope phase, in which the secondary ejects a large amount of hydrogen envelope (Belczynski et al. 2016). The primary BH accretes the common envelope of $\rho \sim 3M_{\text{env}} / (4\pi a^3) \sim 1 \times 10^{-8} \text{ g cm}^{-3}$ for $M_{\text{env}} \sim 30 \text{ M}_\odot$ and $a \sim 10^{14} \text{ cm}$. Using the Bondi-Hoyle-Lyttleton rate, the mass accretion rate is estimated to be $1 \times 10^{28} \text{ g s}^{-1}$, where we use $v \sim \sqrt{GM_{\text{BH}}/a} \sim 6 \times 10^6 \text{ cm s}^{-1}$. Thus, it might be possible to have luminous transients powered by this huge accretion luminosity. Another possibility is from supernova impostors, in which the evolved secondary ejects a large amount of its envelope (Smith et al. 2011). The mass of the ejected material is estimated to be $0.01\text{--}10 \text{ M}_\odot$. Since the accretion rate and the outflow luminosity are proportional to the ejecta mass, the supernova impostors could induce more luminous CIATs than what occurs at the BBH formation.

The spin of the primary BH can also affect the light curves of CIATs. If the primary has a high spin, a rela-

tivistic jet is launched when the primary accretes the ejecta (Blandford & Znajek 1977; Toma & Takahara 2016). If the jet can penetrate the ejecta, GRBs of long duration ($t \sim 10^3 \text{ s}$) and very low-luminosity ($L_{\text{iso}} \sim 10^{47} \text{ erg s}^{-1}$) may be possible.

Other formation channels to form a BBH involve binaries consisting of a BH and a blue supergiant (BSG) (Kinugawa et al. 2014; Inayoshi et al. 2017). However, since the cores of BSGs are very compact, they can eject very little amounts of their outer material, which is unlikely to produce CIATs (Kashiyama, private communication). Red supergiants (RSGs), which also collapse to BHs, can eject large amount of their envelopes ($\gtrsim 1 \text{ M}_\odot$) when collapsing (Lovegrove & Woosley 2013). Thus, it is possible that BH-RSG binaries can also produce CIATs. However, our spherically symmetric treatment would not be accurate for such cases, because of the very large separation ($a > R_* \gtrsim 10^{13} \text{ cm}$).

4. TIDALLY-LOCKED SECONDARY SUPERNOVAE FROM BBH FORMATION (BBH-TLSSNE)

4.1. Optical Emission

We consider a tidally-synchronized binary system where the spin period of the secondary is synchronized to the orbital period of the primary. In this section, we choose $M_* = 10^{1.5} \text{ M}_\odot$ and $R_* = 10^{11} \text{ cm}$ and other parameters are the same as in the previous section. This parameter set satisfies $t_{\text{TL}} \lesssim t_{\text{life}}$ (see Section 2), and is consistent with stellar evolution models (Schaerer & Maeder 1992). The spin angular velocity is synchronized to the orbital motion, which is estimated to be $\omega_s = \sqrt{2GM_*/a^3} \simeq 9.2 \times 10^{-4} M_{*,1.5}^{1/2} a_{12}^{-3/2} \text{ s}^{-1}$. This value is so high that the outer part of the stellar material cannot fall towards the BH directly. Thus, an accretion disk is formed around the newborn BH. This produces a massive outflow, which leads to a TLSSN.

When the secondary collapses, the outer material of the secondary at a cylindrical radius ϖ is at the centrifugal radius, $r_{\text{cf}}(R) = \varpi^4 \omega_s^2 / (GM_R) \approx 2\varpi^4 / a^3$, where $M_R \sim M_*$ is the mass enclosed inside the spherical radius $R = \sqrt{\varpi^2 + z^2}$. Setting $r_{\text{cf}} = 6GM_*/c^2$, we obtain the critical radius for disk formation:

$$R_{\text{cr}} \approx \left(\frac{3GM_* a^3}{c^2} \right)^{1/4} \simeq 6.1 \times 10^{10} M_{*,1.5}^{1/4} a_{12}^{3/4} \text{ cm.} \quad (16)$$

Since $R_* > R_{\text{cr}}$ for our parameter choice, the outer material can form a disk. The density profile of WRs can be expressed as a polytropic sphere of index $\sim 2.5\text{--}3.5$ (Kushnir et al. 2016). The outer region ($R \gtrsim R_*/2$) of a polytrope n can be fitted as $\rho_{\text{env}} \approx \rho_*(R_*/R - 1)^n$ (Matzner & McKee 1999), where $\rho_* \approx A_\rho M_*/(4\pi R_*^3)$, and $A_\rho \simeq 3.9$ are numerical constants that depend on the polytrope index. This expression can reproduce the

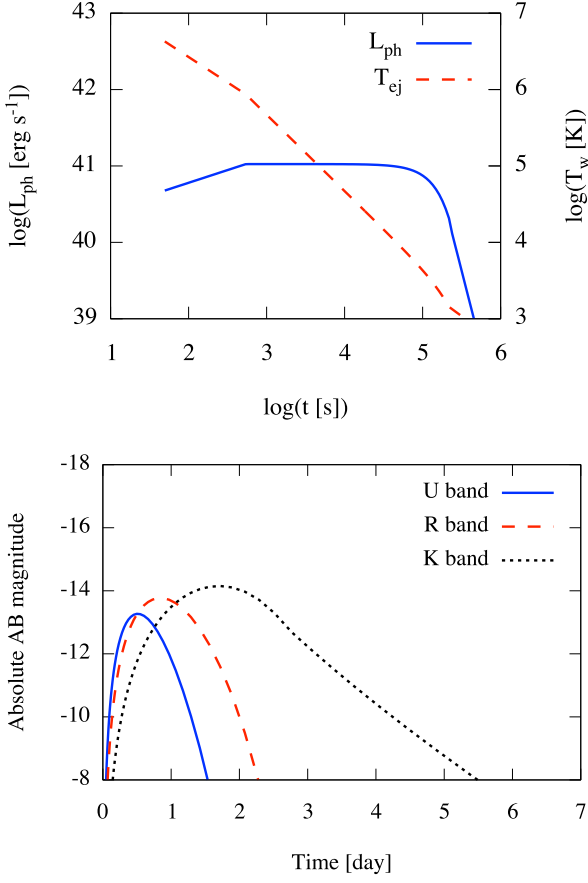


Figure 3. Same as Figure 2, but for the TLSSN and the magnitude in the K band instead of in the UV range. Beyond $t \gtrsim 2.5$ days, our treatment is not accurate.

polytrope within errors of a few percents, except for the very outer edge which does not affect the result. The disk mass is then estimated to be

$$M_d \approx 4\pi \int_{R_{\text{cr}}}^{R_*} d\varpi \int_0^{\sqrt{R_*^2 - \varpi^2}} dz \varpi \rho_* \left(\sqrt{\frac{R_*^2}{\varpi^2 + z^2}} - 1 \right)^n = A_\rho I_d M_* \simeq 0.41 M_{*,1.5} I_{-2.5} M_\odot, \quad (17)$$

where $I_d = \int_{x_{\text{cr}}}^1 dx \int_0^{\sqrt{1-x^2}} dy (1/\sqrt{x^2 + y^2} - 1)^n \simeq 3.3 \times 10^{-3}$ and $x_{\text{cr}} = R_{\text{cr}}/R_*$. Note that I_d is a strong function of x_{cr} that depends on M_* , so that the dependence of M_d on M_* is not simple. The outer material falls to the disk in a free fall time, $t_{\text{ff}} \approx \sqrt{R_*^3/(GM_*)} \simeq 5.4 \times 10^2 M_{*,1.5}^{-1/2} R_{*,11}^{3/2}$ s. Then, the mass accretion rate is estimated to be

$$\dot{M}_{\text{env}} \approx \frac{M_d}{t_{\text{ff}}} \simeq 7.5 \times 10^{-4} M_{*,1.5}^{1/2} R_{*,11}^{-3/2} M_{d,-0.39} M_\odot \text{ s}^{-1}. \quad (18)$$

While this is much larger than the Eddington rate, the neutrino cooling is not efficient (Popham et al. 1999). Thus, the disk state is similar to the case with CIATs, where a strong outflow is produced. The outflow lumi-

nosity is estimated to be

$$L_w \approx \frac{1}{2} \eta_w \dot{M}_{\text{env}} V_w^2 \simeq 2.4 \times 10^{49} M_{*,1.5}^{1/2} R_{*,11}^{-3/2} M_{d,-0.39} \eta_{-0.5} V_{10}^2 \text{ erg s}^{-1}, \quad (19)$$

The duration of the outflow is comparable to the free-fall time, since the accretion time after the disk formation is much shorter than the free-fall time. The total mass of the outflow is $M_w = \eta_w M_d \simeq 0.14 M_{d,-0.39} \eta_{-0.5} M_\odot$ and the total energy is

$$E_w \approx \frac{1}{2} \eta_w M_d V_w^2 \simeq 1.3 \times 10^{52} M_{d,-0.39} \eta_{-0.5} V_{10}^2 \text{ erg}. \quad (20)$$

Since this outflow is much more massive and energetic than the ejecta of failed SNe, we can neglect the effects of the ejecta for $t \gtrsim 10$ s, where $t = 0$ is the time when the outflow begins to be produced.

We assume that the outflow occurs at the escape velocity, and is launched at $r_{\text{lp}} \approx 2GM_*/V_w^2 \simeq 8.4 \times 10^7 M_{*,1.5} V_{10}^{-2}$ cm. Assuming that the radiation energy is comparable to the kinetic energy at the launching point, the temperature at that point is

$$T_{\text{lp}} \approx \left(\frac{\dot{M}_w V_w}{8\pi a_r r_{\text{lp}}^2} \right)^{1/4} \simeq 1.4 \times 10^9 M_{*,1.5}^{-3/8} R_{*,11}^{-3/8} M_{d,-0.39}^{1/4} \eta_{-0.5}^{1/4} V_{10}^{5/4} \text{ K}, \quad (21)$$

where $\dot{M}_w = \eta_w \dot{M}_{\text{env}}$. We assume a constant outflow velocity, which leads to $R \sim V_w t$. For $t < t_{\text{ff}}$, the outflow is continuously produced. Considering adiabatic expansion, we obtain $\rho_w \propto R^{-2}$ and $T_w \propto R^{-2/3}$ where ρ_w and T_w are the density and temperature in the outflow, respectively. The luminosity of the diffusion photons evolves as $L_{\text{ph}} \sim Ra_r T_w^4 / (\kappa \rho_w) \propto R^{1/3}$. At $t = t_{\text{ff}}$, the temperature is

$$T_{\text{ws,t}} \approx T_{\text{lp}} \left(\frac{r_{\text{lp}}}{V_w t_{\text{ff}}} \right)^{2/3} \simeq 8.5 \times 10^5 M_{*,1.5}^{5/8} R_{*,11}^{-11/8} M_{d,-0.39}^{1/4} \eta_{-0.5}^{1/4} V_{10}^{-3/4} \text{ K}. \quad (22)$$

For $t_{\text{ff}} < t$, the outflow expands in a homologous manner. Then, the evolutionary features up to the radiation breakout time are the same as those for CIATs; $\rho_w \propto r^{-3}$, $T_w \propto r^{-1}$, and $L_{\text{ph}} \propto r^0$. The breakout time, the temperature, and the bolometric luminosity for TLSSNe are

$$t_{\text{bo,t}} \approx \sqrt{\frac{\kappa M_w}{4\pi c V_w}} \simeq 1.2 \times 10^5 M_{d,-0.39}^{1/2} \eta_{-0.5}^{1/2} V_{10}^{1/2} \text{ s}. \quad (23)$$

$$T_{\text{bo,t}} \approx T_{\text{ws,t}} \left(\frac{r_{\text{ws,t}}}{R_{\text{bo,t}}} \right) \simeq 4.0 \times 10^3 M_{*,1.5}^{1/8} R_{*,11}^{1/8} M_{d,-0.39}^{-1/4} \eta_{-0.5}^{-1/4} V_{10}^{-1/4} \text{ K}, \quad (24)$$

$$L_{\text{ph}} \approx \frac{4\pi R_{\text{bo,t}}^3 a_r T_{\text{bo,t}}^4}{3\kappa t_{\text{bo,t}}} \simeq 1.1 \times 10^{41} M_{*,1.5}^{1/2} R_{*,11}^{1/2} V_{10} \text{ erg s}^{-1}, \quad (25)$$

where $R_{\text{bo,t}} = V_w t_{\text{bo,t}}$. For $t > t_{\text{bo,t}}$, the internal energy decreases due to the escape of radiation. Since V_w is close to the speed of light, the outflow becomes optically thin soon. At $t \gtrsim t_{\text{thin}} \simeq 2.2 \times 10^5$ s $\simeq 2.5$ days, using $t_{\text{ph}} \sim v_w t/c$, we obtain $\mathcal{E}_{\text{int}} \propto t^{-c/V_w}$. Accordingly, T_w and L_{ph} would show a rapid decline after $\sim t_{\text{thin}}$. Our treatment with the approximate use of the Planck distribution would become inaccurate, especially at $\tau \lesssim 1 - 10$. To study the features of decay phase, a more careful treatment of thermalization processes would be required (see also the Section 4.3 and 5).

The evolution of T_w and L_{ph} are shown in the upper panel of Figure 3. The lower panel of the figure shows the evolution of the absolute AB magnitude in the U , R , and K (2 μm) bands. TLSSNe have low magnitudes, short durations, and red colors, compared to CIATs. Again, assuming that the event rate of TLSSNe is similar to the merger rate of BBHs, the expected distance is around 200 Mpc, implying apparent magnitudes of $\sim 23 - 24$. Thus, it may not be easy to detect TLSSNe with current optical transient surveys such as PTF, Pan-STARRS, and KISS, but LSST would be able to detect them. Their shorter duration and fainter bolometric luminosities are useful for distinguishing TLSSNe from the usual SNe. They could also be distinguished from macronovae/kilonovae using the helium lines, as is the case for CIATs (see Section 3).

Interestingly, $t_{\text{bo,t}}$, $T_{\text{bo,t}}$, and $L_{\text{bo,t}}$ do not have a strong dependence on the parameters. However, the occurrence of TLSSNe is sensitive to the value of $x_{\text{cr}} = R_{\text{cr}}/R_* \simeq 0.61 M_{*,1.5}^{1/4} R_{*,11}^{-1} a_{12}^{3/4}$. For $x_{\text{cr}} > 1$, an accretion disk is not formed, which leads to a similar result as in Section 3. For $x_{\text{cr}} \ll 1$, a significant fraction of the stellar material falls onto the disk, and the primary BH has a large spin, resulting in a GRB.

4.2. Radio afterglow

Outflow-driven transients may lead to radio afterglows (see Kashiyama et al. 2017 for details; see also Murase et al. 2016). We briefly discuss this possibility here (cf. Chevalier 1998; Nakar & Piran 2011, for supernovae and neutron star mergers). The deceleration radius and time is estimated to be

$$R_{\text{dec}} \approx \left(\frac{3M_w}{4\pi n_{\text{ext}} m_p} \right)^{1/3} \quad (26)$$

$$\simeq 5.0 \times 10^{18} M_{d,-0.39}^{1/3} \eta_{-0.5}^{1/3} n_{-1}^{-1/3} \text{ cm},$$

$$t_{\text{dec}} \approx \frac{R_{\text{dec}}}{V_w} \simeq 5.0 \times 10^8 M_{d,-0.39}^{1/3} \eta_{-0.5}^{1/3} V_{10}^{-1} n_{-1}^{-1/3} \text{ s}, \quad (27)$$

where $n_{\text{ext}} = 0.1 n_{-1} \text{ cm}^{-3}$ is the number density of the circum-binary medium. After the deceleration time, the evolution of the outflow is represented by the self-similar solution,

$$R = R_{\text{dec}} (t/t_{\text{dec}})^{2/5} (t \geq t_{\text{dec}}), \quad (28)$$

$$V = 0.4 V_w (t/t_{\text{dec}})^{-3/5} (t \geq t_{\text{dec}}). \quad (29)$$

We estimate physical quantities around $t \sim t_{\text{dec}}$ using $V \sim V_w$ and $R \sim R_{\text{dec}}$. The magnetic field is estimated to be $B = (9\pi m_p n_{\text{ext}} \epsilon_B v^2) \simeq 1.4 V_{10} n_{-1}^{1/2} \epsilon_{-2}^{1/2} \text{ mG}$, where ϵ_B is the energy fraction of the magnetic field. The minimum Lorentz factor of electrons is estimated to be

$$\gamma_m \approx \zeta_e \left(\frac{m_p}{m_e} \right) \left(\frac{v}{c} \right)^2 \simeq 1.2 \times 10^2 V_{10}^2 \zeta_{-0.4}, \quad (30)$$

where $\zeta_e \sim (p-2)\epsilon_e/((p-1)f_e) \sim 0.4$, ϵ_e is the energy fraction of the non-thermal electrons, $f_e \sim 0.1$ is the number fraction of non-thermal electron, and p is the spectral index of the non-thermal electrons. The cooling Lorentz factor is $\gamma_c \approx 6\pi m_e c / (\sigma_T B^2 t_{\text{dec}}) \simeq 7.4 \times 10^5 M_{d,-0.39}^{-1/3} \eta_{-0.5}^{-1/3} V_{10}^{-1} n_{-1}^{-2/3} \epsilon_{-2}^{-1}$, where σ_T is the Thomson cross section. Since $\gamma_m \ll \gamma_c$, the synchrotron spectrum in the slow cooling regime. The synchrotron frequencies for the electrons of γ_m and γ_c are

$$\nu_m \approx \frac{\gamma_m^2 e B}{2\pi m_e c} \simeq 6.0 \times 10^7 V_{10}^5 n_{-1}^{1/2} \epsilon_{-2}^{1/2} \zeta_{-0.4}^2 \text{ Hz.} \quad (31)$$

$$\nu_c \simeq 2.2 \times 10^{15} M_{d,-0.39}^{-2/3} \eta_{-0.5}^{-2/3} V_{10}^{-3} n_{-1}^{-5/6} \epsilon_{-2}^{-3/2} \text{ Hz.} \quad (32)$$

If we ignore synchrotron self absorption (SSA), the synchrotron spectrum has a peak at ν_m and its flux is

$$F_{\nu,m} \approx \frac{P_m N_e}{4\pi \nu_m d_L^2} \quad (33)$$

$$\simeq 22 M_{d,-0.39} \eta_{-0.5} V_{10} n_{-1}^{1/2} \epsilon_{-2}^{1/2} f_{-1} d_{27}^{-2} \text{ mJy,}$$

where $P_m \approx \gamma_m^2 \sigma_T c B^2 / (6\pi)$ is the power of synchrotron radiation per electron, $N_e \approx 4\pi R^3 n_{\text{ext}} f_e / 3$ is the total non-thermal electron number, and $d_L \simeq 10^{27}$ cm is the luminosity distance. Since $F_{\nu} \propto \nu^{(1-p)/2}$ for $\nu_m < \nu < \nu_c$ without SSA, the observed flux at frequency ν_{obs} is estimated to be

$$F_{\nu,\text{obs}} \approx F_{\nu,m} \left(\frac{\nu_{\text{obs}}}{\nu_m} \right)^{(1-p)/2} \simeq 1.3 \nu_9^{\frac{1-p}{2}} M_{d,-0.39} \times \eta_{-0.5} V_{10}^{\frac{5p-3}{2}} n_{-1}^{\frac{p+1}{4}} \epsilon_{-2}^{\frac{p+1}{4}} f_{-1} d_{27}^{-2} \text{ mJy,} \quad (34)$$

where we use $p = 3$ to estimate the value. Since the sensitivity of current radio surveys is around 0.1 mJy, it is possible to detect this radio emission. Using Equations (28) and (29), we obtain $F_{\nu,\text{obs}} \propto t^3$ for $t < t_{\text{dec}}$ and $F_{\nu,\text{obs}} \propto t^{(21-15p)/10}$ for $t > t_{\text{dec}}$. Note that $F_{\nu,\text{obs}}$ has a strong dependence on V_w , $F_{\nu,\text{obs}} \propto V_w^6$ for $p = 3$.

Thus, just a few times lower V_w would make it difficult to detect the radio afterglow.

The optical depth for SSA is estimated to be $\tau_a \approx A_p e f_e n_{\text{ext}} R (\nu / \nu_m)^{-(p+4)/2} / (B \gamma_m^5)$, where A_p is a function of p ($A_p = 26.31$ for $p = 3$, see [Murase et al. \(2014\)](#)). The SSA frequency at which $\tau_a = 1$ is estimated to be

$$\nu_a \approx \left(A_p \frac{e f_e n_{\text{ext}} R}{B \gamma_m^5} \right)^{2/(p+4)} \nu_m \simeq 1.3 \times 10^8 M_{d,-0.39}^{\frac{2}{p+4}} \times \eta_{-0.5}^{\frac{2}{p+4}} V_{10}^{\frac{5p-2}{p+4}} n_{-1}^{\frac{3p+14}{6p+24}} \epsilon_{-2}^{\frac{p+2}{2p+8}} \xi_{-0.4}^{\frac{2p-2}{p+4}} f_{-1}^{\frac{2}{p+4}} \text{ Hz.} \quad (35)$$

This frequency evolves $\nu_a \propto t^{2/(p+4)}$ for $t < t_{\text{dec}}$ and $\nu_a \propto t^{-(3p+2)/(p+4)}$ for $t > t_{\text{dec}}$ ([Nakar & Piran 2011](#)). If we focus on $\nu_{\text{obs}} > \nu_a$, we can ignore the effect of SSA. Since we typically expect $\nu_a > \nu_m$, the spectrum is modified by SSA as $F_\nu \propto \nu^{5/2}$ for $\nu_m < \nu < \nu_a$ and $F_\nu \propto \nu^2$ for $\nu < \nu_m$.

4.3. Some TLSSN Caveats

Since the mass accretion rate is large enough, we expect some nucleosynthesis around the secondary BHs, producing radioactive nuclei ([Pruet et al. 2003](#); [Fujimoto et al. 2004](#)). If the outflow contains $\gtrsim 0.01 M_\odot$ of Ni^{56} , this could affect the light curves in the decay phase, which would probably change the color of the TLSSNe to bluer than our estimate.

Since BSGs and RSGs have larger radii than WRs, $x_{\text{cr}} < 1$ is easily satisfied. In this sense, TLSSNe are likely in BH-BSG and BH-RSG binaries. However, whether the spin is tidally synchronized or not depends strongly on the internal structure of the secondary ([Kushnir et al. 2016](#)). More accurate modeling will require solving the stellar evolution in detail, which remains as future work.

5. CONCLUSION

We investigated two types of outflow-driven transients from newborn binary black holes formed from BH-WR binaries, within the context of isolated binary evolution scenarios. One type is a companion-induced accretion transient onto the primary BH (CIATs), and the other type occurs in tidally locked systems (TLSSNe), both leading to weak SN-like events.

In the former scenario, when the secondary collapses to a BH, it ejects a fraction of the outer material of the secondary. Part of the ejecta accretes onto the primary BH, and the accretion rate can exceed the Eddington rate, owing to the high density of the ejecta. As a result, the primary BH produces an outflow which injects a significant amount of energy into the unaccreted ejecta. This powers a CIAT whose kinetic energy reaches $\sim 10^{48}$ ergs for optimistic parameters. The bolometric luminosity of this transients can be $\sim 10^{40} - 3 \times 10^{41} \text{ erg s}^{-1}$,

and the U -band absolute magnitude ranges from ~ -10 to ~ -12 , with a duration of around a week.

In the latter scenario, we consider the tidally synchronized binaries, which are likely to occur in close and massive binaries. In this case, the outer material of the collapsing secondary forms a disk around the secondary BH. This also results in an energetic outflow of kinetic energy $\sim 10^{52}$ ergs, leading to a TLSSN whose bolometric luminosity can be $\sim 10^{40} - 10^{41} \text{ erg s}^{-1}$. Its R -band absolute magnitude reaches ~ -13 , with a duration of a few days. One could distinguish both of these outflow-driven transients from usual SNe and macronovae/kilonovae by shorter duration, lower bolometric luminosities, and strong helium lines.

A caveat is that we used a one-zone approximation to estimate the light curves. In reality, the physical quantities have a radial dependence which may complicate the features of these transients. Also the circum-binary medium is possibly polluted by material ejected by a stellar wind, ejection of the common envelope and/or supernova impostors, which could affect the light curves. Atomic recombination processes may also modify the light curves when the ejecta cools down to a few 10^4 K.

These transients leave an accretion disk around a BH in a BBH, which a few years later becomes neutral due to radiative cooling, thus naturally creating a fossil disk in which the angular momentum transport is inefficient, e.g. [Perna et al. \(2014, 2016\)](#); [Kimura et al. \(2017\)](#). This fossil disk can remain for millions of years until the BBH merges, resulting in the possible electromagnetic counterparts of GWs from BBHs ([Murase et al. 2016](#); [Kimura et al. 2017](#)).

We expect an event rate for these SNe similar to the LIGO event rate, $\sim 9 - 240 \text{ Gpc}^{-3} \text{ yr}^{-1}$ ([Abbott et al. 2016a](#)). We expect $\sim 0.1 - 2$ events within 200 Mpc in a year, which leads to the peak apparent magnitudes of $\sim 24 - 25$ for CIATs, and $\sim 23 - 24$ for TLSSNe. Thus, future observations with, e.g., the Large Synoptic Survey Telescope (LSST, [LSST Science Collaboration et al. 2009](#)), may be able to detect these outflow-driven transients. We caution that the event rate of CIATs and TLSSNe have uncertainties. Since the separation distribution in binaries is $\propto a^{-1}$ ([Abt 1983](#)), although the wide binaries with WRs are faint, the wide binaries with different progenitor (BSG or RSG) may increase the event rate. Also, the star formation rate is higher for higher redshift, so we could expect that the BBH formation rate has the same tendency ([Kinugawa et al. 2014](#); [Inayoshi et al. 2016](#)). In this case, the event rate in the local universe is likely to be lower than the GW rate.

CIATs and TLSSNe can be distinguished from usual SNe by their weaker peak luminosity and shorter light curves, and (also unlike macronovae/kilonovae)

by their strong helium lines. Recently, rapid transients of timescale around a day to a week are observed (Drout et al. 2014; Tanaka et al. 2016). Although the timescale of the observed transients are comparable to our predictions, our models predicts much lower magnitudes than the observed ones.

These new transients can also produce radiation in other wavelengths as well. For the early part of the homologously expanding phase, both models have temperatures $\sim 10^6$ K with $L_{\text{ph}} \sim 10^{41}$ erg s $^{-1}$, which results in fluxes of $\sim 10^{-13}$ erg s $^{-1}$ around 0.2 keV with duration $\sim 10^3$ s for $d_L \sim 100$ Mpc (where d_L is the luminosity distance). This could be detectable by the extended ROentgen Survey with an Imaging Telescope Array (eROSITA; Merloni et al. 2012). For CIATs, a shock breakout (cf. Matzner & McKee 1999) at $t \sim t_{\text{dur}}$ is possible, which is likely to have a higher flux and higher peak energy with shorter duration than the soft X-ray

emission above. Another counterpart is radio emission from the TLSSNe, as discussed in Section 4. For CIATs, the radio emission is very weak, due to low V_{ej} .

In conclusion, we have discussed two new possible types of bright electromagnetic transients which occur at the time when a binary black hole system forms, which could be detectable by future optical surveys, and which can be distinguished from other transients via their characteristic luminosities and light curves.

The authors thank Kazumi Kashiyama, Kunihito Ioka, and Tomoya Kinugawa for useful comments. This work is partially supported by NSF Grant No. PHY-1620777 (K.M.), NASA NNX13AH50G (S.S.K. and P.M.), and by an IGC post-doctoral fellowship program (S.S.K.).

REFERENCES

Abbott, B. P. et al. 2016a, *Physical Review X*, 6, 041015
 — 2016b, *Physical Review Letters*, 116, 241103
 — 2016c, *Physical Review Letters*, 116, 061102
 Abt, H. A. 1983, *ARA&A*, 21, 343
 Bartos, I., Kocsis, B., Haiman, Z., & Márka, S. 2017, *ApJ*, 835, 165
 Belczynski, K., Holz, D. E., Bulik, T., & O’Shaughnessy, R. 2016, *Nature*, 534, 512
 Blandford, R. D. & Znajek, R. L. 1977, *MNRAS*, 179, 433
 Bondi, H. 1952, *MNRAS*, 112, 195
 Chevalier, R. A. 1998, *ApJ*, 499, 810
 Crowther, P. A. 2007, *ARA&A*, 45, 177
 Dai, L., McKinney, J. C., & Miller, M. C. 2016, *ArXiv e-prints*:1611.00764
 de Val-Borro, M., Karovska, M., & Sasselov, D. 2009, *ApJ*, 700, 1148
 Detmers, R. G., Langer, N., Podsiadlowski, P., & Izzard, R. G. 2008, *A&A*, 484, 831
 Dominik, M., Belczynski, K., Fryer, C., Holz, D. E., Berti, E., Bulik, T., Mandel, I., & O’Shaughnessy, R. 2012, *ApJ*, 759, 52
 Drout, M. R. et al. 2014, *ApJ*, 794, 23
 Edgar, R. 2004, *New Astron. Rev.*, 48, 843
 Fujimoto, S.-i., Hashimoto, M.-a., Arai, K., & Matsuba, R. 2004, *ApJ*, 614, 847
 Hashizume, K., Ohsuga, K., Kawashima, T., & Tanaka, M. 2015, *PASJ*, 67, 58
 Hodapp, K. W. et al. 2004, *Astronomische Nachrichten*, 325, 636
 Hotokezaka, K. & Piran, T. 2017, *ArXiv e-prints*:1702.03952
 Hoyle, F. & Lyttleton, R. A. 1939, *Proceedings of the Cambridge Philosophical Society*, 35, 405
 Huarte-Espinosa, M., Carroll-Nellenback, J., Nordhaus, J., Frank, A., & Blackman, E. G. 2013, *MNRAS*, 433, 295
 Inayoshi, K., Hirai, R., Kinugawa, T., & Hotokezaka, K. 2017, *ArXiv e-prints*:1701.04823
 Inayoshi, K., Kashiyama, K., Visbal, E., & Haiman, Z. 2016, *MNRAS*, 461, 2722
 Ioka, K., Matsumoto, T., Teraki, Y., Kashiyama, K., & Murase, K. 2016, *ArXiv e-prints*:1612.03913
 Jiang, Y.-F., Stone, J. M., & Davis, S. W. 2014, *ApJ*, 796, 106
 Kasen, D. & Bildsten, L. 2010, *ApJ*, 717, 245
 Kashiyama, K. & Quataert, E. 2015, *MNRAS*, 451, 2656
 Kimura, S. S., Takahashi, S. Z., & Toma, K. 2017, *MNRAS*, 465, 4406
 Kimura, S. S., Toma, K., & Takahara, F. 2014, *ApJ*, 791, 100
 Kinugawa, T., Inayoshi, K., Hotokezaka, K., Nakauchi, D., & Nakamura, T. 2014, *MNRAS*, 442, 2963
 Kushnir, D., Zaldarriaga, M., Kollmeier, J. A., & Waldman, R. 2016, *MNRAS*, 462, 844
 Law, N. M. et al. 2009, *PASP*, 121, 1395
 Li, L.-X. & Paczyński, B. 1998, *ApJ*, 507, L59
 Loeb, A. 2016, *ApJ*, 819, L21
 Lovegrove, E. & Woosley, S. E. 2013, *ApJ*, 769, 109
 LSST Science Collaboration et al. 2009, *ArXiv e-prints*:0912.0201
 Mandel, I. & de Mink, S. E. 2016, *MNRAS*, 458, 2634
 Mandic, V., Bird, S., & Cholis, I. 2016, *Physical Review Letters*, 117, 201102
 Marchant, P., Langer, N., Podsiadlowski, P., Tauris, T. M., & Moriya, T. J. 2016, *A&A*, 588, A50
 Matzner, C. D. & McKee, C. F. 1999, *ApJ*, 510, 379
 Merloni, A. et al. 2012, *ArXiv e-prints*:1209.3114
 Moriya, T., Tominaga, N., Tanaka, M., Nomoto, K., Sauer, D. N., Mazzali, P. A., Maeda, K., & Suzuki, T. 2010, *ApJ*, 719, 1445
 Morokuma, T. et al. 2014, *PASJ*, 66, 114
 Murase, K., Kashiyama, K., Mészáros, P., Shoemaker, I., & Senno, N. 2016, *ApJ*, 822, L9
 Murase, K., Thompson, T. A., & Ofek, E. O. 2014, *MNRAS*, 440, 2528
 Nadezhin, D. K. 1980, *Ap&SS*, 69, 115
 Nakamura, T., Sasaki, M., Tanaka, T., & Thorne, K. S. 1997, *ApJ*, 487, L139
 Nakar, E. & Piran, T. 2011, *Nature*, 478, 82
 Narayan, R., Sadowski, A., & Soria, R. 2017, *ArXiv e-prints*:1702.01158
 Ohsuga, K., Mori, M., Nakamoto, T., & Mineshige, S. 2005, *ApJ*, 628, 368
 Paczynski, B. 1976, in *IAU Symposium*, Vol. 73, *Structure and Evolution of Close Binary Systems*, ed. P. Eggleton, S. Mitton, & J. Whelan, 75
 Perna, R., Duffell, P., Cantiello, M., & MacFadyen, A. I. 2014, *ApJ*, 781, 119
 Perna, R., Lazzati, D., & Giacomazzo, B. 2016, *ApJ*, 821, L18

Popham, R., Woosley, S. E., & Fryer, C. 1999, *ApJ*, 518, 356

Portegies Zwart, S. F. & McMillan, S. L. W. 2000, *ApJ*, 528, L17

Pruet, J., Woosley, S. E., & Hoffman, R. D. 2003, *ApJ*, 586, 1254

Rodriguez, C. L., Haster, C.-J., Chatterjee, S., Kalogera, V., & Rasio, F. A. 2016, *ApJ*, 824, L8

Sasaki, M., Suyama, T., Tanaka, T., & Yokoyama, S. 2016, *Physical Review Letters*, 117, 061101

Sadowski, A., Narayan, R., McKinney, J. C., & Tchekhovskoy, A. 2014, *MNRAS*, 439, 503

Schaerer, D. & Maeder, A. 1992, *A&A*, 263, 129

Shima, E., Matsuda, T., Takeda, H., & Sawada, K. 1985, *MNRAS*, 217, 367

Sigurdsson, S. & Hernquist, L. 1993, *Nature*, 364, 423

Smith, N., Li, W., Silverman, J. M., Ganeshalingam, M., & Filippenko, A. V. 2011, *MNRAS*, 415, 773

Stone, N. C., Metzger, B. D., & Haiman, Z. 2017, *MNRAS*, 464, 946

Takahara, F. & Kusunose, M. 1985, *Progress of Theoretical Physics*, 73, 1390

Takahashi, H. R. & Ohsuga, K. 2015, *PASJ*, 67, 60

Takahashi, H. R., Ohsuga, K., Kawashima, T., & Sekiguchi, Y. 2016, *ApJ*, 826, 23

Tanaka, M. et al. 2016, *ApJ*, 819, 5

Tassoul, J.-L. 1987, *ApJ*, 322, 856

Toma, K. & Takahara, F. 2016, *Progress of Theoretical and Experimental Physics*, 2016, 063E01

Tutukov, A. V. & Yungelson, L. R. 1993, *MNRAS*, 260, 675

Webbink, R. F. 1984, *ApJ*, 277, 355

Yoon, S.-C., Woosley, S. E., & Langer, N. 2010, *ApJ*, 725, 940

Zahn, J.-P. 1977, *A&A*, 57, 383